

Polydopamine reinforced hemostasis of a graphene oxide sponge via enhanced platelet stimulation

Guofeng Li^{a,*}, Yuping Liang^a, Congcong Xu^a, Hui Sun^b, Lei Tao^c, Yen Wei^c, Xing Wang^{a,*}

^a The State Key Laboratory of Chemical Resource Engineering, Beijing Laboratory of Biomedical Materials, Beijing Advanced Innovation Center for Soft Matter Science and Engineering, Beijing University of Chemical Technology, Beijing 100029, PR China

^b Tongliao Infectious Disease Hospital, Tongliao, 028000, PR China

^c Department of Chemistry and the Tsinghua Center for Frontier Polymer Research, Tsinghua University, Beijing, 100084, PR China

ARTICLE INFO

Keywords:

Dopamine
DCGO
Graphene oxide
Hemostatic sponge
Hemostasis

ABSTRACT

Graphene oxide (GO) is a promising hemostatic material because of its platelet stimulatory activity. However, our previous studies on cross-linked graphene sponges demonstrated that those sponges lost the GO function of platelet stimulation due to the pristine GO was reduced under the harsh reaction conditions. Accordingly, a mild cross-linking strategy is expected to preserve the oxygen-containing groups to further increase the hemostatic performance of the sponges. Here, we present a polydopamine (PDA) cross-linked GO sponge (DCGO) by using mild and facile wet chemistry. The obtained DCGO possessed a high surface charge (-31.3 ± 0.3 mV) and showed strong platelet stimulation. Moreover, this method strengthened the mechanical properties of the DCGO, which supported 350 times its own weight without deformation, thus ensuring its absorbability. For the synergy of platelet stimulation and physical absorption, DCGO achieved outstanding hemostatic performance. Bleeding stopped within 105 ± 15 s, which was 165 s faster than that of the un-cross-linked GO aerogel and 96 s faster than that of the cross-linked graphene sponge (CGS). The DCGO combines the advantages of both PDA and GO, thus supplying a new material and method for the field of trauma hemostasis.

1. Introduction

Graphene oxide (GO) is a precursor of graphene that has great potential in biomedical fields, such as drug delivery, cancer therapy, biosensing, cellular imaging and antibacterial surfaces [1–6]. Recently, GO nanosheets were reported to activate platelets and then elicit their strong aggregate response because of the abundant oxygen-containing functional groups of the nanosheet [7–10]. When platelets are activated, they can carry many other hemostatic factors, adhere to a wound and trigger the coagulation pathway. This property is similar to that of coagulation stimulation-type agents, such as chitosan and thrombin [11,12]. However, this function of platelet stimulation is lost when GO is reduced. Singh et al reported that reduced GO (rGO) is not endowed with any prothrombotic or platelet-stimulating characteristics because of the loss of oxygen-containing groups [13]. Our previous studies on graphene-based sponges also confirmed that those sponges lost the GO function of platelet stimulation [14–18], which was mainly due to the removal of most of the oxygen groups from the GO surface under the harsh reaction conditions. Accordingly, a mild cross-linking strategy may be more favorable for preserving the oxygen functional groups and

maintaining the stimulatory effect on platelets. For example, poly(vinyl alcohol) cross-linked GO aerogel achieves coagulation and acts as a drug delivery system [19]. Therefore, a mild cross-linking strategy is expected to improve the hemostatic performance of GO-based sponges by increasing platelet stimulation by GO.

Dopamine (DOPA) is one of the main mussel foot proteins and represents a pivotal factor for mussel adhesion and cohesion. The catechols in DOPA have an exceptionally versatile reaction chemistry that is responsible for attaching to different inorganic/organic surfaces. Catechols can also be converted to quinones, further participating in cross-linking and sclerotization [20]. Therefore, DOPA is widely used as a coating agent and strength enhancer [21–26]. Recently, a graphene/DOPA composite has attracted much scientific and engineering interest. Through self-polymerization, covalent interactions, and π - π stacking, DOPA easily combines with graphene-based materials and effectively enhances their tensile strength and toughness [27–29]. A previous study showed that a DOPA/GO composite exhibits 1.5–2 times higher strength than the natural nacre [27]. Additionally, DOPA can also be used in tissue-adhesive hydrogels and improves tissue-adhesive and hemostatic properties due to its strong binding strength, high

* Corresponding authors.

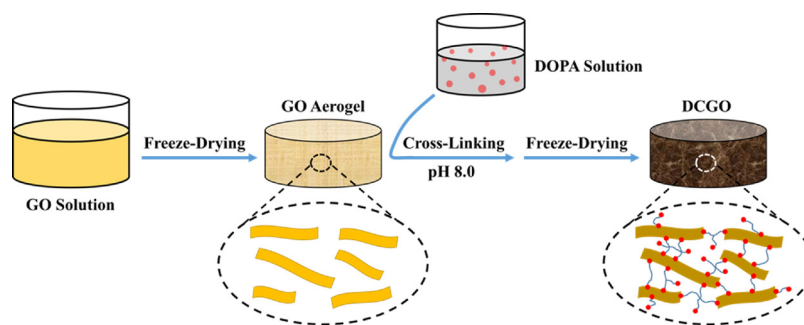
E-mail addresses: chase.lg@163.com (G. Li), wangxing@mail.buct.edu.cn (X. Wang).

<https://doi.org/10.1016/j.colsurfb.2018.10.074>

Received 17 May 2018; Received in revised form 28 September 2018; Accepted 25 October 2018

Available online 02 November 2018

0927-7765/ © 2018 Elsevier B.V. All rights reserved.



Scheme 1. Schematic of the preparation of the DCGO. The un-cross-linked GO aerogel was immersed in an alkaline solution in which DOPA self-polymerized through alkali-induced polymerization and modified the surface of the GO aerogel simultaneously. After freeze-drying, the DCGO was obtained.

toughness, and tissue biocompatibility [30–32]. Therefore, these studies confirmed that a DOPA cross-linked network could increase the mechanical strength of GO sponges and prevent the leakage of GO nanosheets. Furthermore, the mild self-polymerization reaction of DOPA may preserve the oxygen groups in the GO-based composite sponges when compared with the abovementioned strict cross-linking strategy.

In this study, we present a polydopamine (PDA) cross-linked GO hemostatic sponge (DCGO) produced via wet chemistry, in which DOPA self-polymerizes under basic conditions and modifies the surface of the un-cross-linked GO aerogel simultaneously (Scheme 1). The oxygen functional groups of the DCGO increase under the mild reaction conditions and exhibit platelet-stimulating characteristics. In addition, the self-polymerization of DOPA forms a cross-linked network that strengthens the mechanical properties of the DCGO. The strong mechanical properties improve the absorbability of the DCGO. As such, for the synergistic effect of platelet stimulation and physical absorption, the DCGO is expected to be an effective trauma hemostat.

2. Experiments

2.1. Materials

DOPA and tris(hydroxymethyl)aminomethane (Tris) were purchased from Sigma. Sprague-Dawley (SD) rats were purchased from Vital (Charles) River Laboratory, Beijing, China. Fresh blood was obtained from the SD rats, and anticoagulant (ACD) whole blood was obtained by combining fresh blood and citrate dextrose at the ratio of 9:1. Other commonly used chemical reagents were purchased commercially.

All SD rats used for the animal experiments in this study were treated and cared for in accordance with the National Research Council's Guide.

2.2. Preparation and characterization of the DCGO

2.2.1. Material preparation

Preparation of the DCGO. A volume of 20 mL GO solution (8 mg/mL, obtained according to the literature [33]) was placed in a 50 mL beaker and freeze dried for 48 h to obtain the GO aerogel. A volume of 30 mL Tris-HCl buffer (pH = 8.0) containing 10 μ M DOPA was slowly added to the beaker until the GO aerogel was submerged. DOPA self-polymerized through an alkali-induced polymerization process and cross-linked the GO aerogel. After reacting for 12 h and removing the excess solution, the DCGO was freeze dried for another 48 h. The obtained DCGO was purified by multiple alcohol soaking steps (repeated 4 times, for 6 h each time).

2.2.2. Characterization of the DCGO

A scanning electron microscope (SEM, Hitachi S-4700) was used to observe the morphology of the DCGO. A gas sorption analyzer

(Quantachrome, Autosorb IQ) was used to investigate the pore size distribution and the surface area of the DCGO. Attenuated total reflection Fourier transformed infrared spectroscopy (ATR-FTIR, PerkinElmer, Spectrum 100) and element analysis (EA, Vario Elcube) were used to investigate the chemical composition of the DCGO. X-ray diffraction (XRD, D/Max 2500 VB2+/PC) and Raman spectroscopy (RENISHAW InVia) were used to analyze the structure of the DCGO. The zeta potential (Malvern NanoSizer ZS2000) was used to detect the negative potential of the DCGO.

The absorption ability was investigated by calculating the weight difference between the initial weight of the DCGO and the weight after adequately absorbing the liquid. The absorption rate was recorded with a high-speed camera (40 ms per frame).

The mechanical strength of the un-cross-linked GO aerogel and the DCGO was tested. First, deformation after absorbing water was assessed. A droplet of water was dropped on the GO aerogel or the DCGO, and then the morphology of the materials was recorded by a camera. Second, the deformation after loading weight was evaluated. Weight was loaded on the surface of the materials, and after 30 s, the morphology of the materials was recorded by a camera.

2.3. Blood cell evaluations

2.3.1. Select adhesion of blood cells or platelets

First, the anticoagulant (ACD) rat whole blood was prepared by mixing fresh rat blood and citrate dextrose at a 9:1 ratio. The platelet rich plasma (PRP) was the supernatant of the ACD-whole blood and was obtained by centrifugation at $2000 \times g$ for 20 min at 4 $^{\circ}$ C.

A piece of the DCGO ($1 \times 1 \text{ cm}^2$) was equilibrated in 20 mL of phosphate buffer solution (PBS) for 2 h at 37 $^{\circ}$ C. Then, 1 mL of ACD-whole blood or 2 mL of PRP was added and allowed full contact for 1 h at 37 $^{\circ}$ C. PBS was added 3 times to remove the blood cells or PRP that did not adhere to the DCGO. Then, the material was immobilized with 2.5% glutaraldehyde for 2 h and immersed in a gradient of ethanol (50%, 60%, 70%, 80%, 90% and 100%) for 10 min. The sample was freeze dried and metal sprayed before the SEM observations.

2.3.2. Morphological study of the blood cells

The ACD rat whole blood or PRP was directly dropped on the surface of the DCGO. After 3 min, excess PBS was used to rinse the free blood cells or PRP 3 times. Then, the material was immobilized with 2.5% glutaraldehyde for 2 h and immersed in a gradient of ethanol (50%, 60%, 70%, 80%, 90% and 100%) for 10 min. The sample was freeze dried and metal sprayed before performing SEM observations (S-4700 Hitachi).

2.3.3. Quantitative analysis of platelet adhesion

The research method was performed according to a previous study [7]. Platelets extracted from fresh rat blood (2×10^8 cells in 200 μ L PBS) were incubated with the DCGO (2 μ g/mL) or thrombin (200 μ L, 1 U/mL) at 37 $^{\circ}$ C for 20 min and then fixed with 4% paraformaldehyde at

4 °C for 2 h. The cells were cultured onto slides coated with fibrinogen (100 µg/mL), incubated for 30 min at room temperature, and then washed. The adhered cells were observed under a microscope. The spread area of platelets treated by the DCGO has been quantified using the software of ImageJ. 50 platelet cells were randomly selected to calculate their average area.

2.3.4. Dynamic blood clotting test with ACD human blood

The tested samples (control, the DCGO and 10 U thrombin) were placed at the bottoms of 5 mL beakers. The beakers were placed in a thermostat at 37 °C for 5 min, and 100 µL ACD whole blood was dropped on the surface of these materials, followed by the addition of 10 µL CaCl₂ solution (0.2 mol/L) to the blood sample. The beakers containing blood sample were kept in a thermostat at 37 °C for 5 min. The blood clotting test was carried out by spectrophotometric measurement of the relative absorbency of blood sample that had been diluted by 25 mL distilled water at 540 nm. The absorbency of solution of 25 mL distilled water and 100 µL human ACD whole blood at 540 nm was assumed to be 100, which was used as reference value. That is to say, the blood clotting index (BCI) of biomaterial can be quantified by the following equation:

$$\text{BCI} = (\text{Absorbency of blood contacted with sample}) / (\text{Absorbency of solution of distilled water and ACD blood}).$$

2.4. Rat tail amputation test

Approximately 7-week-old male SD rats were housed for 3 days in a standard environment before operation. The rats were anesthetized with 10% chloral hydrate (w/v) at a ratio of 0.5 mL per 100 g. The rat tail was cut at approximately 8 cm of the total length. Then, the sponge material was pressed on the wound section, and the bleeding time was recorded.

3. Results and discussion

3.1. Material characterization

Fig. 1A shows a typical DCGO hemostatic sponge prepared via PDA modification of the un-cross-linked GO aerogel. PDA worked as an adhesive that firmed the GO aerogel without destroying its architecture. Thus, this composite sponge perfectly exhibited the architectural features of the GO aerogel, such as a fluffy and small porous structure

(Fig. 1B). Fig. 1C shows an SEM image of the porous cavity interior structure in the DCGO. Large numbers of honeycomb-like channels can be clearly observed, and the cell walls of the channels are smooth via the adhesion of PDA (Fig. 1D). The pores of the DCGO sponge were analyzed by N₂ adsorption-desorption isotherms. According to the IUPAC classification, the curves of the un-cross-linked GO aerogel and the DCGO were assigned to type IV with an H3 hysteresis loop at a relative pressure P/P₀ [33,34]. An analysis of the BJH pore size distributions (Fig. 2A) showed that the GO aerogel contained a broad peak for the adsorption pore diameter, which ranged from 3 to 10 nm. For the DCGO, the BJH pore size was mainly 10 nm, and the smaller pores were blocked with PDA. With the addition of PDA, the calculated BET surface area of the DCGO decreased to 16.0 m²/g compared with 22.4 m²/g for the GO aerogel.

ATR-FTIR was performed to identify the chemical structure of the DCGO and the un-cross-linked GO aerogel (Fig. 2B). For the GO aerogel, the peaks at 3260, 1726, 1620, 1428, and 1075 cm⁻¹ were attributed to the O–H stretching band, C=O stretching vibration, C=C stretching vibration of sp² hybridization, C–OH bending vibration, and C–O–C stretching vibration, respectively [35–37]. After cross-linking with PDA, the obtained DCGO exhibited the functional groups of GO and the typical absorption peaks of PDA. New peaks emerged at 2937, 1508, and 1367 cm⁻¹ and could be assigned to the C–H stretching band in the CH₂ group, N–H scissoring vibration, and phenolic O–H bending, respectively. The intensity of the absorption peaks at 1620 and 1075 cm⁻¹ increased because of the amino and phenol groups in the PDA [36,38]. These results indicated that the PDA/GO composite was prepared successfully.

The DCGO structure was investigated by Raman spectroscopy. As shown in Fig. 2C, the GO aerogel and DCGO had similar Raman peaks, such that the G peak was at approximately 1593 cm⁻¹ and the D peak was at 1358 cm⁻¹. The D peak and the G peak represented the structural defects and first-order scattering of the E2g mode, respectively. The integral area ratio (ID/IG) of the GO aerogel was approximately 1.0, whereas the DCGO increased to 1.2. Additionally, the full width at half-maximum of the G-band value of the DCGO decreased from 109 cm⁻¹ to 97 cm⁻¹, indicating the restoration of the sp² hybridized carbon network of graphene [39]. These results were consistent with that of a previous study in which the electrons released during the oxidative polymerization of DOPA were shown to remove part of the oxygen functional groups of the GO aerogel by coupling the oxidation and reduction processes [40,41]. Accordingly, the degree of reduction of the

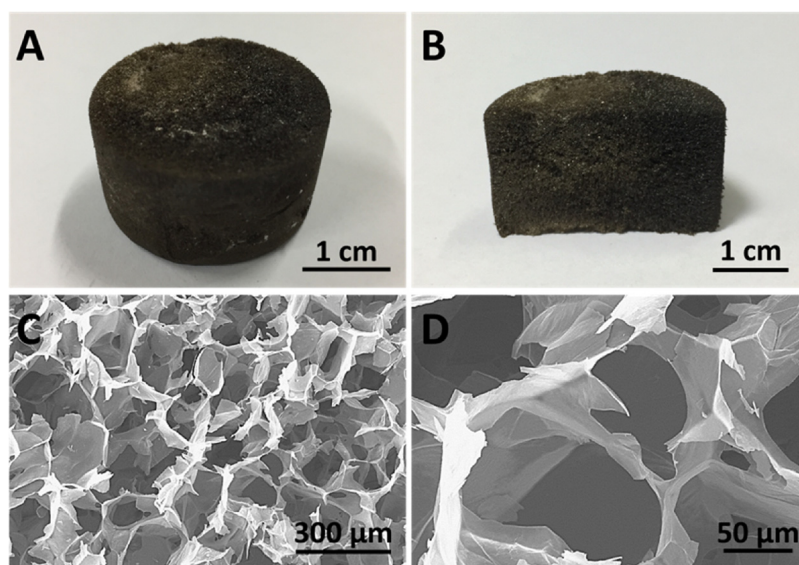


Fig. 1. (A) Photograph of the DCGO (2.6 cm diameter, 1.5 cm thickness). (B) Cross section of the DCGO. (C) SEM image of the interior porous structure. (D) Smooth cell wall of the porous structure.

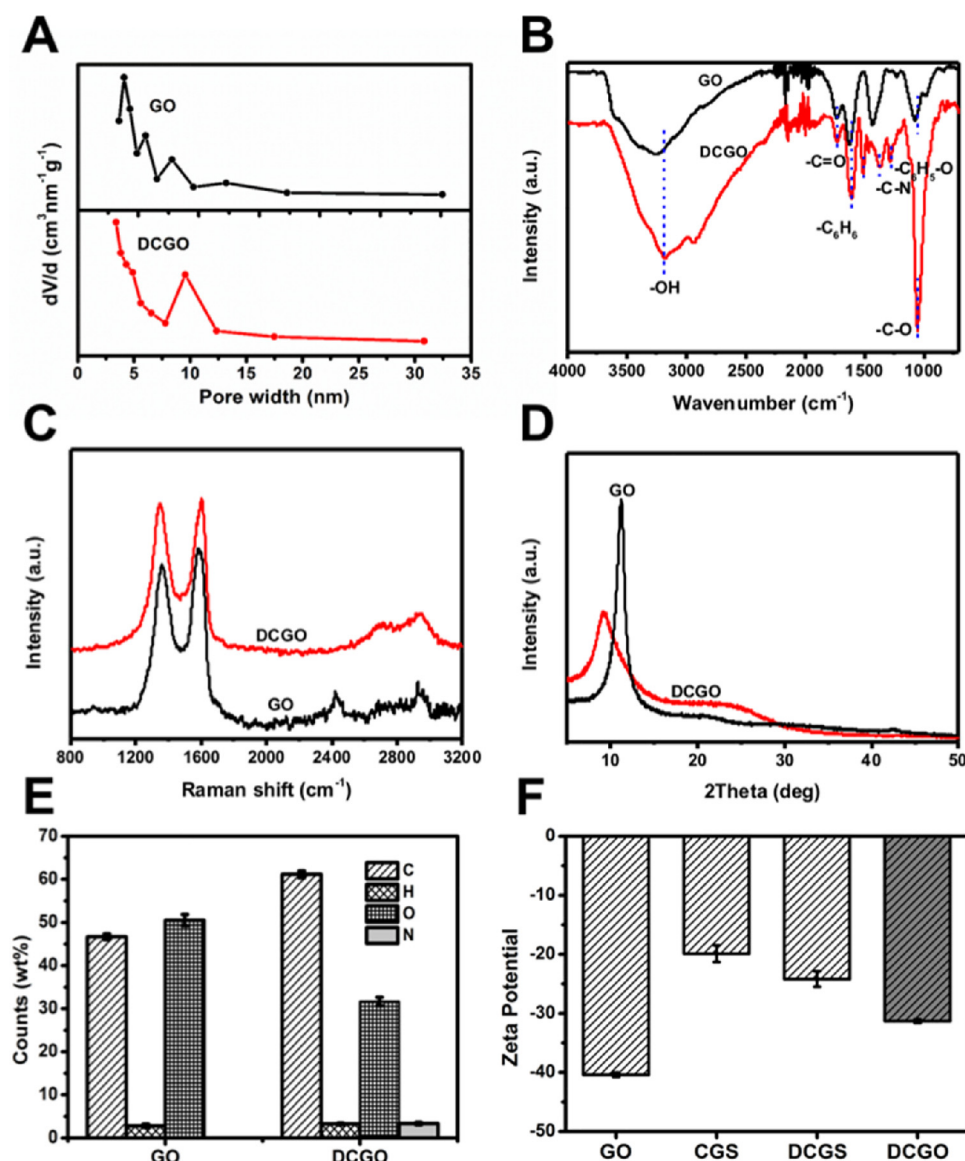


Fig. 2. Characterization of the DCGO. (A) BJH pore size distribution of the DCGO and un-cross-linked GO aerogel. (B) ATR-FTIR, (C) Raman, (D) XRD and (E) EA of the DCGO and GO aerogel. (F) Zeta potential tests of the DCGO, GO aerogel, CGS and DCGS. Data values correspond to the mean \pm SD, $n = 5$.

DCGO was further investigated by XRD measurements. As shown in Fig. 2D, the GO aerogel had a typical diffraction peak at $2\theta = 11^\circ$ ($d = 0.80$ nm). When the GO aerogel was cross-linked by PDA, the interlayer spacing was enlarged via the insertion of PDA. Thus, the diffraction peak of the DCGO shifted to $2\theta = 9^\circ$ ($d = 0.98$ nm). In addition, a new peak was observed at $2\theta = 25^\circ$ ($d = 0.35$ nm) in the DCGO. This peak was weak, suggesting that many oxygen-containing groups may remain in the DCGO.

To further confirm the presence of oxygen functional groups, the element content of the DCGO was assessed by EA analysis (Fig. 2E). The content of N elements was approximately 3.3%, and it was introduced by PDA. The content of C elements in the DCGO increased from 46.7% to 61.2%, whereas the O elements decreased from 50.5% to 31.7%. The C/O mass ratio of the DCGO presented an enhancement from 0.7 to 1.4, thus indicating the reduction reaction of the DCGO. However, carbon is the main element of PDA. The introduction of PDA would also increase the C/O mass ratio of the DCGO. Nevertheless, these results demonstrated that the oxygen contained in the DCGO was high and favored induction of the charge stimulation of platelets.

The zeta potential test confirmed the high surface charges of the DCGO (Fig. 2F). The negative electric potential of the DCGO was

approximately -31.3 ± 0.3 mV. Although lower than the GO aerogel (-40.4 ± 0.4 mV), the DCGO showed a higher negative charge density than our other reported materials, the cross-linked graphene sponge (CGS) and DapA cross-linked graphene sponge (DCGS). The electric negative potentials of the CGS and DCGS were -19.9 mV and -24.2 mV, respectively [14,15]. The results confirmed that this mild preparation strategy is more beneficial for increasing the oxygen functional groups of the DCGO. The higher negative charge may give the DCGO strong stimulatory properties for platelets and enhances its hemostatic performance.

3.2. Interaction with blood cells

Therefore, with the aim of clarifying whether the DCGO composite can activate platelets, morphological studies of the hemocytes and platelets on the surface of the DCGO were performed according to our previous method [14–16]. As shown in Fig. 3A, when the DCGO was incubated with ACD rat whole blood in PBS, blood cells adhered on the surface of the DCGO and maintained their original morphology. By contrast, when the DCGO was incubated with PRP, we clearly observed a larger number of proteins covering the surface of the DCGO. Platelets

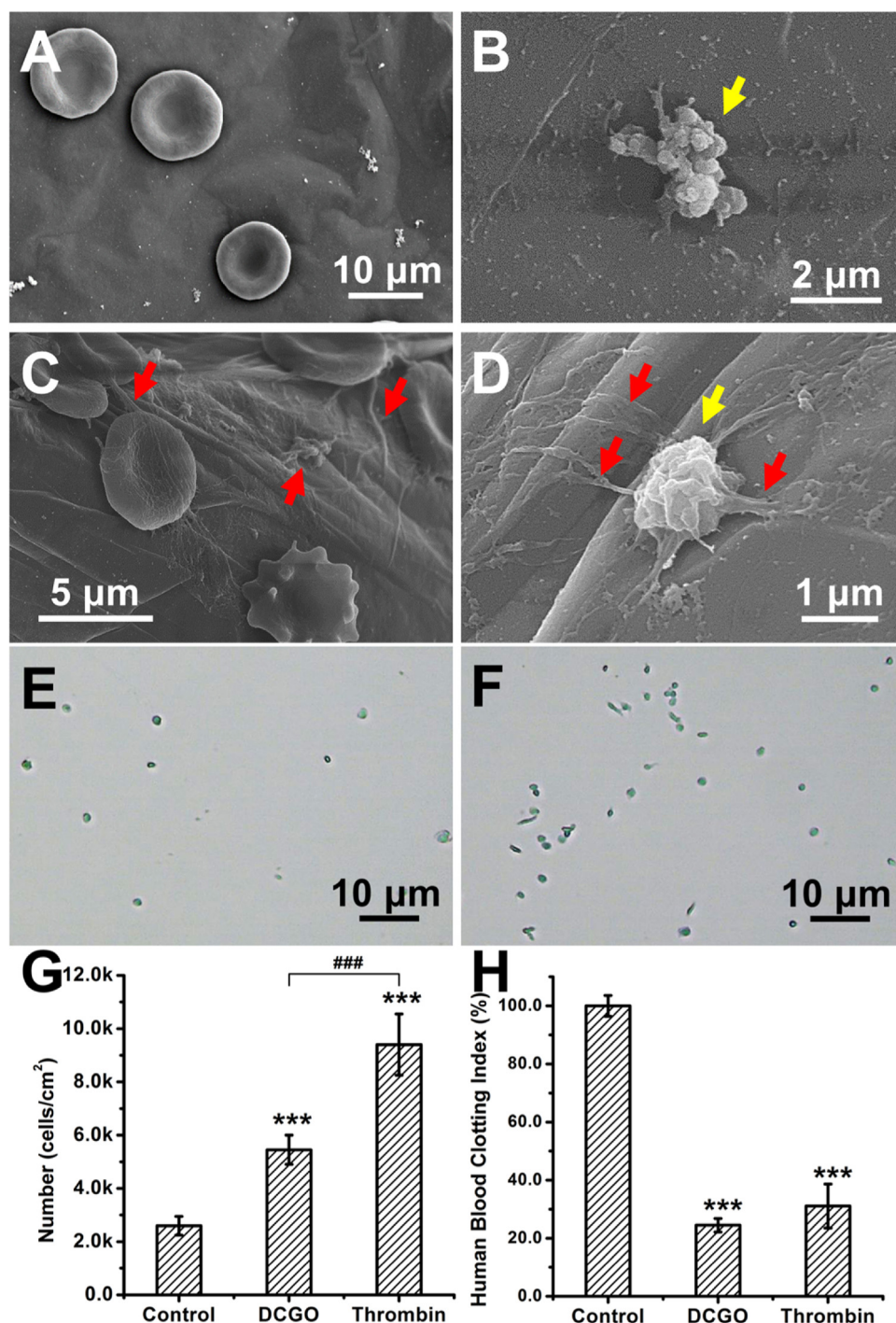


Fig. 3. Interaction between blood cells and the DCGO. Selective adsorption of (A) rat blood cells and (B) platelets. (C) Fibrin formed when whole blood was directly dropped onto the DCGO. (D) Platelets were active when PRP was directly dropped onto the DCGO. The red and yellow arrows show the fibrin and active platelet, respectively. Adhesion and spreading of platelets on immobilized fibrinogen. (E) Untreated platelets. (F) DCGO (2 $\mu\text{g/mL}$). (G) Statistical analysis of the number of pretreated cells adhered onto the fibrinogen matrix. (H) ACD Human blood clotting index of DCGO and thrombin (10 U). Data values correspond to the mean \pm SD, $n = 6$. Two-way ANOVA; *** and ### indicate $p < 0.001$, and *** represents a significant difference when compared with the control groups (For interpretation of the references to colour in this figure legend, the reader is referred to the web version of this article).

aggregated on the surface and changed their regular shape (Fig. 3B). However, in our previous study, the platelets attached to the CGS surface maintained a regular resting shape because of the reduction in GO [14]. Because the DCGO directly contacted blood during the hemostatic process, the morphology of the blood cells was also observed when a droplet of rat whole blood was dropped onto the DCGO surface. Plasma was quickly absorbed into the DCGO, leaving a larger number of blood cells aggregated on the surface of the DCGO and forming a micron-sized blood clot. In the topical field, a few blood cells were observed (Fig. 3C). Compared with the blood cells incubated in PBS, the blood cells directly dropped onto the DCGO surface were covered and cross-linked by the formed fibrin (red arrows in Fig. 3C). The presence of red blood cells during clot formation increased the fibrin network

heterogeneity and strengthened the clot stability [42]. Moreover, when PRP was dropped onto the DCGO surface, platelets were activated. As shown in Fig. 3D, the platelets were bound to fibrin and displayed a pseudopodia-like morphology. These activated platelets could support a burst of thrombin generation on the surface. The produced thrombin sequentially triggered fibrinogen, which converted to a stable fibrin clot [43,44]. The quantitative analysis of platelet adhesion to the DCGO was further studied. Platelets pretreated with DCGO (2 $\mu\text{g/mL}$) or thrombin (1 U/mL) were cultured onto slides coated with fibrinogen. Because of the interaction between activated platelets and fibrinogen, the DCGO-pretreated platelets exhibited enhanced adhesion to fibrinogen (Fig. 3E and 3F). Thrombin-pretreated platelets, as a positive control, showed the strongest adhesion to fibrinogen. Nevertheless, the adhered number

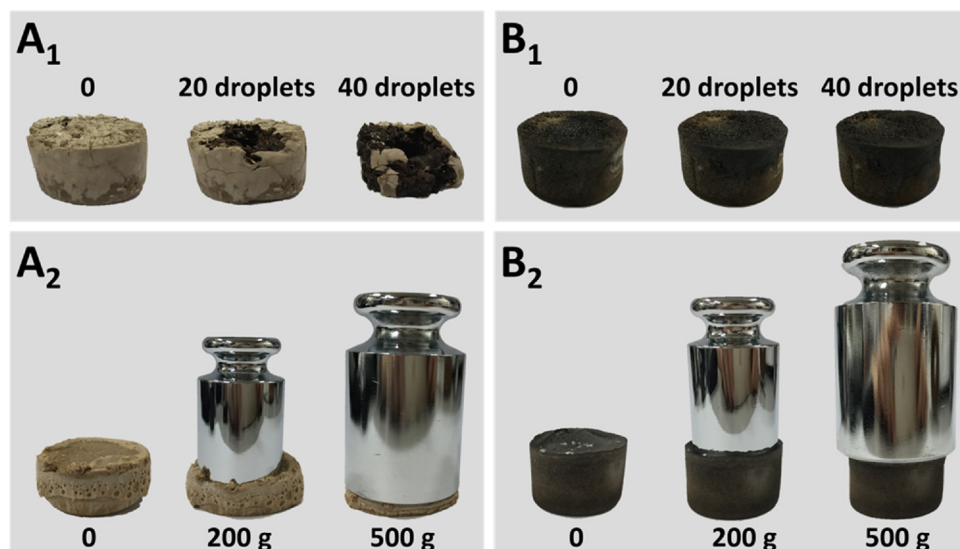


Fig. 4. Mechanical strength of the un-cross-linked GO aerogel and DCGO. Deformation of (A) the GO aerogel and (B) the DCGO after (A₁, B₁) dropping water or (A₂, B₂) loading with weight. The deformation of (A₁) the GO aerogel and (B₁) the DCGO after absorbing 20 and 40 droplets of water. The deformation of (A₂) the GO aerogel and (B₂) the DCGO after loading 200 and 500 g of weight.

and spread area of the DCGO-pretreated cells were over twice than those of the nontreated cells (Fig. 3G), indicating the platelet-activated effect of the DCGO. Considering that rodent blood is different from human blood, the dynamic blood clotting test with human blood was also investigated. As shown in Fig. 3H, the human blood clotting index of the DCGO was consistent with that of 10 U thrombin. They were significantly lower than that of the blank, suggesting that the DCGO could effectively enhance human blood clotting. Therefore, these results demonstrated that the DCGO is an effective agonist for activating platelets and has great potential in hemostasis.

3.3. Mechanical strength and absorption capability

Mechanical strength is another important factor for affecting the hemostasis of the GO-based sponge. The un-cross-linked GO aerogel has a weak brittle network that inhibits its absorbability and compressibility and thus is not conducive to hemostatic performance. As such, PDA was used as a cross-linker to prevent the leakage of GO nanosheets and enhance the sponge's mechanical strength. As shown in Fig. 4A₁, the GO aerogel lost its shape when it absorbed water. After absorbing 40 droplets of water, the GO aerogel completely collapsed, whereas the DCGO was self-supported. Dropping water on the DCGO did not change its shape. The DCGO could absorb a large quantity of water while maintaining its original shape (Fig. 4B₁). Interestingly, during the preparation of the DCGO, the GO aerogel maintained its structure when added to the DOPA solution, which was mainly because the GO aerogel adhered to the inner wall of the beaker prevented its collapse. Moreover, PDA worked as a strong adhesive to reinforce the strength of the sponge's framework. A weight of 500 g, which was 350 times heavier than the DCGO, could stand on the surface of the DCGO without destroying the shape of the DCGO, whereas the GO aerogel was compressed, even when loaded with only 200 g of weight (Fig. 4A₂ and B₂). These phenomena demonstrated that these mussel-derived polymers can efficiently strengthen the mechanical properties of the DCGO.

By introducing PDA, the obtained DCGO possessed outstanding absorption capabilities. The DCGO could absorb 48.8 ± 1.3 times its own weight of water and 37.1 ± 0.8 times that of blood (Fig. 5). Clearly, the absorption amount of blood was decreased by 24.0% compared with water, which was because the DCGO promoted blood clotting and the formed clot plugged its inner space. This phenomenon indicated that the DCGO should favor hemostasis. The liquid absorption rate of the DCGO was recorded with a high-speed camera. The DCGO had an ultrafast absorption rate and completely absorbed a droplet of water/blood within 120 ms. This feature is vital for stopping bleeding.

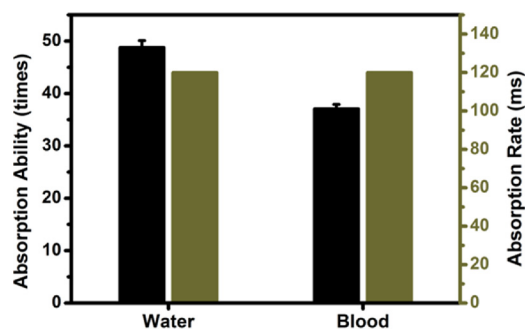


Fig. 5. Water/blood absorption capability and rate of the DCGO. Data values correspond to the mean \pm SD, $n = 5$.

3.4. In vivo Hemostatic efficacy

Rat tail cutting models are a common and mature bleeding model for assessing trauma hemostatic materials [45,46]. Therefore, the hemostatic performance of DCGO was evaluated using this model. After cutting approximately an 8 cm length of the total rat tail, the rat tail artery showed serious hemorrhaging, and the bleeding could not be stopped within 10 min without treatment. However, when the DCGO was slightly compressed onto the wound (Fig. 6A), the DCGO quickly absorbed the blood and rapidly stopped the bleeding. The data statistics (Fig. 6B) revealed that the DCGO stopped the bleeding within 105 ± 15 s ($n = 6$), which was 60 s and 165 s faster than the traditional hemostat montmorillonite (165 ± 52 s, $n = 6$) and the un-cross-linked GO aerogel (270 ± 12 s, $n = 6$), respectively. The total blood loss in the DCGO group was approximately 0.9 ± 0.5 g, whereas the total blood loss in the GO aerogel group was 4.0 ± 0.7 g. These results indicated that the DCGO possessed outstanding hemostatic performance and was significantly better than the GO aerogel. Although the GO aerogel can stimulate platelets, its poor mechanical properties restricted its plasma absorption. As a result, the GO aerogel did not perform well in stopping bleeding. Simultaneously, the hemostatic performance of the other DCGOs prepared using different DOPA concentrations ($5 \mu\text{M}$ for the DCGO₂ and $2.5 \mu\text{M}$ for the DCGO₃) was investigated. Although the DCGO₂ and the DCGO₃ showed a faster liquid absorption rate than the DCGO (80 ms for the DCGO₂ and 40 ms for the DCGO₃), the hemostatic time of the DCGO₂ and the DCGO₃ was lengthened to 135 ± 15 s ($n = 6$) and 150 ± 9 s ($n = 6$), respectively. We propose that the mechanical strength of the DCGO₂ and the DCGO₃ affected their hemostasis. During the hemostatic process, these two

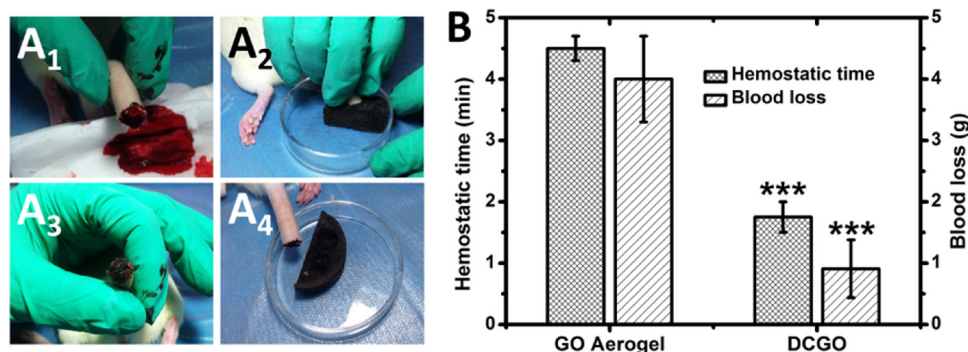


Fig. 6. Evaluation on the hemostatic performance of the DCGO. (A) Hemostatic experiment in a rat tail amputation model. (A₁) Rat tail was cut, and the wound caused hemorrhaging. (A₂) DCGO pressed on the wound. (A₃) Hemostasis was achieved by the DCGO. (A₄) DCGO after hemostatic performance. (B) Data on the hemostasis time and blood loss from rat tail amputation between the DCGO and the un-cross-linked GO aerogel. Data values correspond to the mean \pm SD, $n = 6$. Two-way ANOVA; *** means $p < 0.001$ and represents a significant difference compared with the GO aerogel.

materials deformed significantly after absorbing blood. These results demonstrated that the mechanical strength was important for the hemostasis of the DCGOs. Ensuring the absorption capacity of the DCGO was critical to achieving rapid hemostasis. Moreover, the surface charge density also played an important role in enhancing the hemostasis of the DCGO. Because of the higher charge density, the DCGO showed more advantages in hemostatic performance compared with the previously assessed hemostatic materials, CGS (201 ± 46 s) and DCGS (166 ± 52 s) [14,15]. Therefore, these results indicated that the PDA cross-linked method is a facile and mild strategy for enhancing the hemostatic performance of a graphene-based sponge by improving its mechanical strength and increasing platelet stimulation.

4. Conclusions

In summary, we developed a DCGO hemostatic sponge with PDA modification of a GO aerogel. The mild self-polymerization of DOPA increased the degree of oxidation of DCGO, which exhibited a high surface charge (-31.3 ± 0.3 mV) and effectively activated platelets and accelerated the formation of fibrin. Moreover, the PDA network enhanced the mechanical strength of the DCGO, which was able to support 350 times its own weight without deformation. This strong mechanical property endowed the DCGO with good absorbability. The water (blood) absorption amount of the DCGO was 48.8 ± 1.3 (37.1 ± 0.8), and it completely absorbed a droplet of water/blood within 120 ms. Thus, for the synergy effect of strong platelet stimulation and fast physical absorption, the DCGO showed outstanding hemostatic performance and was able to stop the bleeding within 105 ± 15 s, which was 165 s faster than the performance of the GO sponge (270 ± 12 s). Moreover, the DCGO was also more effective than the CGS (201 ± 46 s) and DCGS (166 ± 52 s) because of its enhanced platelet stimulation. Therefore, this facile and mild cross-linking method is an effective strategy for improving the hemostatic efficiency of graphene-based sponges. The DCGO combines the advantages of PDA and GO and presents great potential in the field of trauma hemostasis.

Acknowledgments

The authors thank the National Natural Science Foundation of China (21574008) and the Fundamental Research Funds for the Central Universities (BHYC1705B and PYBZ1806) for their financial support. Xing Wang also gratefully acknowledges the China Scholarship Council for their financial support on a Visiting Scholar Program (No. 201706885008).

References

- [1] D.R. Dreyer, S. Park, C.W. Bielawski, R.S. Ruoff, *Chem. Soc. Rev.* 39 (2010) 228–240.
- [2] D.C. Marcano, D.V. Kosynkin, J.M. Berlin, A. Sinitskii, Z. Sun, A. Slesarev, L.B. Alemany, W. Lu, J.M. Tour, *ACS Nano* 4 (2010) 4806–4814.

- [3] K.P. Loh, Q. Bao, G. Eda, M. Chhowalla, *Nat. Chem.* 2 (2010) 1015–1024.
- [4] D. Chen, H. Feng, J. Li, *Chem. Rev.* 112 (2012) 6027–6053.
- [5] G. Li, H. Zhao, J. Hong, K. Quan, Q. Yuan, X. Wang, *Colloids Surf. B Biointerfaces* 160 (2017) 220–227.
- [6] X. Zhang, J. Yin, C. Peng, W. Hu, Z. Zhu, W. Li, C. Fan, Q. Huang, *Carbon* 49 (2011) 986–995.
- [7] S.K. Singh, M.K. Singh, M.K. Nayak, S. Kumari, S. Shrivastava, J.J. Grácio, D. Dash, *ACS Nano* 5 (2011) 4987–4996.
- [8] S. Kumari, M.K. Singh, S.K. Singh, J.J. Grácio, D. Dash, *Nanomedicine* 9 (2014) 427–440.
- [9] W. Siess, *Physiol. Rev.* 69 (1989) 58–178.
- [10] A. Hellem, P. Owren, *Acta Haematol.* 31 (1964) 230–238.
- [11] N. Howe, B. Cherpelis, *J. Am. Acad. Dermatol.* 69 (2013) 659.e1 – 659.e17.
- [12] R. Gu, W. Sun, H. Zhou, Z. Wu, Z. Meng, X. Zhu, Q. Tang, J. Dong, G. Dou, *Biomaterials* 31 (2010) 1270.
- [13] S.K. Singh, M.K. Singh, P.P. Kulkarni, V.K. Sonkar, J.J. Grácio, D. Dash, *ACS Nano* 6 (2012) 2731–2740.
- [14] K. Quan, G. Li, D. Luan, Q. Yuan, L. Tao, X. Wang, *Colloids Surf. B Biointerfaces* 132 (2015) 27–33.
- [15] K. Quan, G. Li, L. Tao, Q. Xie, Q. Yuan, X. Wang, *ACS Appl. Mater. Interfaces* 8 (2016) 7666–7673.
- [16] G. Li, K. Quan, Y. Liang, T. Li, Q. Yuan, L. Tao, Q. Xie, X. Wang, *ACS Appl. Mater. Interfaces* 8 (2016) 35071–35080.
- [17] G. Li, K. Quan, C. Xu, B. Deng, X. Wang, *Colloids Surf. B Biointerfaces* 161 (2018) 27–34.
- [18] Y. Liang, C. Xu, G. Li, T. Liu, J.F. Liang, X. Wang, *Colloids Surf. B Biointerfaces* 169 (2018) 168–175.
- [19] C. Mellado, T. Figueroa, R. Baez, R. Castillo, M. Melendrez, B. Schulz, K. Fernandez, *ACS Appl. Mater. Interfaces* 10 (2018) 7717–7729.
- [20] M. Krogsgaard, V. Nue, H. Birkedal, *Chem.–Eur. J.* 22 (2016) 844–857.
- [21] M.E. Lyngre, R. van der Westen, A. Postma, B. Städler, *Nanoscale* 3 (2011) 4916–4928.
- [22] Y. Liu, K. Ai, L. Lu, *Chem. Rev.* 114 (2014) 5057–5115.
- [23] R. Batul, T. Tamanna, A. Khaliq, A. Yu, *Biomater. Sci.* 5 (2017) 1204–1229.
- [24] X. Zhang, S. Wang, L. Xu, L. Feng, Y. Ji, L. Tao, S. Li, Y. Wei, *Nanoscale* 4 (2012) 5581–5584.
- [25] X. Zhang, K. Wang, M. Liu, X. Zhang, L. Tao, Y. Chen, Y. Wei, *Nanoscale* 7 (2015) 11486–11508.
- [26] M. Liu, G. Zeng, K. Wang, Q. Wan, L. Tao, X. Zhang, Y. Wei, *Nanoscale* 8 (2016) 16819–16840.
- [27] W. Cui, M. Li, J. Liu, B. Wang, C. Zhang, L. Jiang, Q. Cheng, *ACS Nano* 8 (2014) 9511–9517.
- [28] X. Song, L. Lin, M. Rong, Y. Wang, Z. Xie, X. Chen, *Carbon* 80 (2014) 174–182.
- [29] W. Lee, J.U. Lee, B.M. Jung, J.-H. Byun, J.-W. Yi, S.-B. Lee, B.-S. Kim, *Carbon* 65 (2013) 296–304.
- [30] Y. Liu, H. Meng, Z. Qian, N. Fan, W. Choi, F. Zhao, B.P. Lee, *Angew. Chem., Int. Ed.* 56 (2017) 4224–4228.
- [31] Y.C. Choi, J.S. Choi, Y.J. Jung, Y.W. Cho, *J. Mater. Chem. B* 2 (2014) 201–209.
- [32] L. Han, L. Yan, K. Wang, L. Fang, H. Zhang, Y. Tang, Y. Ding, L.-T. Weng, J. Xu, J. Weng, *NPG Asia Mater.* 9 (2017) e372.
- [33] G. Li, X. Wang, L. Tao, Y. Li, K. Quan, Y. Wei, L. Chi, Q. Yuan, *J. Membr. Sci.* 495 (2015) 439–444.
- [34] B. Shen, D. Lu, W. Zhai, W. Zheng, *J. Mater. Chem. C* 1 (2013) 50–53.
- [35] M. Sookhakian, Y.M. Amin, W.J. Basirun, *Appl. Surf. Sci.* 283 (2013) 668–677.
- [36] M. Li, X. Huang, C. Wu, H. Xu, P. Jiang, T. Tanaka, *J. Mater. Chem.* 22 (2012) 23477–23484.
- [37] X. Zhang, W. Hu, J. Li, L. Tao, Y. Wei, *Toxicol. Res.* 1 (2012) 62–68.
- [38] M. Zhang, X. Zhang, X. He, L. Chen, Y. Zhang, *Nanoscale* 4 (2012) 3141–3147.
- [39] X. Wu, J. Zhou, W. Xing, G. Wang, H. Cui, S. Zhuo, Q. Xue, Z. Yan, S.Z. Qiao, *J. Mater. Chem.* 22 (2012) 23186–23193.
- [40] J.-Y. Hong, X. Yu, B.M. Bak, C. Pang, H.S. Park, *Carbon* 83 (2015) 71–78.
- [41] W. Li, T. Shang, W. Yang, H. Yang, S. Lin, X. Jia, Q. Cai, X. Yang, *ACS Appl. Mater. Interfaces* 8 (2016) 13037–13050.
- [42] S. Kattula, J.R. Byrnes, A.S. Wolberg, *Arterioscler. Thromb. Vasc. Biol.* 37 (2017) E13–E21.
- [43] M.R. de Queiroz, B.B. de Sousa, D.F. da Cunha Pereira, C.C.N. Mamede, M.S. Matias, N.C. Gomes de Moraes, Jd.O. Costa, F. de Oliveira, *Toxicol. Clin.* 133 (2017) 33–47.
- [44] M. Hoffman, D.M. Monroe, *Hematol. Oncol. Clin. N* 21 (2007) 1–11.
- [45] J. van Ryn, J. Schurer, M. Kink-Eiband, A. Clemens 118 (2011) 2316.
- [46] J. Jin, Z. Ji, M. Xu, C. Liu, X. Ye, W. Zhang, S. Li, D. Wang, W. Zhang, J. Chen, F. Ye, Z. Lv, *ACS Biomater. Sci. Eng.* 4 (2018) 2541–2551.